

# Demonstration of InAs/InGaAs/GaAs Quantum Dots-in-a-well Mid-wave Infrared Photodetectors Grown on Silicon Substrate

Wei Chen,\* Zhuo Deng,\* Daqian Guo, Yaojiang Chen, Yuriy I. Mazur, Yurii Maidaniuk, Mourad Benamara, Gregory J. Salamo, Huiyun Liu, Jiang Wu, and Baile Chen

**Abstract**—In this work, we have demonstrated the first InAs/InGaAs/GaAs quantum dots-in-a-well (DWELL) photodetector monolithically grown on silicon substrate. We studied both the optical and electrical characteristics of the DWELL photodetectors. Time-resolved photoluminescence spectra measured from the DWELL photodetector revealed a long carrier lifetime of 1.52 ns. A low dark current density of  $2.03 \times 10^{-3}$  mA/cm<sup>2</sup> was achieved under 1 V bias at 77 K. The device showed a peak responsivity of 10.9 mA/W under 2 V bias at the wavelength of 6.4  $\mu$ m at 77 K, and the corresponding detectivity was  $5.78 \times 10^8$  cm<sup>2</sup>·Hz<sup>1/2</sup>/W. These results demonstrated that these silicon based DWELL photodetectors are very promising for future mid-infrared applications, which can enjoy the potential benefit from mid-infrared silicon photonics technology.

**Index Terms** — infrared photodetector, quantum dots-in-a-well, silicon substrate.

## I. INTRODUCTION

Mid-wave infrared (MWIR) photodetectors have many applications in areas such as gas monitoring, chemical sensing, and infrared imaging [1-3]. Traditional bulk photodetectors like mercury-cadmium-telluride (MCT), while they have been demonstrated with high responsivity and specific detectivity, they still suffer from material non-uniformity, problems related to epitaxial growth of mercury-based compounds, and the relatively high cost of the CdZnTe substrate [4, 5].

Quantum wells infrared photodetectors (QWIPs), which utilize

This work was supported in part by the Shanghai Sailing Program under Grant 17YF1429300, in part by the ShanghaiTech University startup funding under Grant F-0203-16-002, in part by the UK EPSRC First Grant EP/R006172/1 and in part by the National Science Foundation under Grant EPSCoR Grant # OIA-1457888. (Corresponding authors: Jiang Wu and Baile Chen.)

W. Chen is with the Shanghai Institute of Microsyst & Information Technology, Shanghai 200050, Chinese Academy of Sciences, Peoples R China; Optoelectronic Device Laboratory, School of Information Science & Technology, ShanghaiTech University, Shanghai 201210, Peoples R China; University of Chinese Academy of Sciences, Peoples R China (e-mail: [chenwei@shanghaitech.edu.cn](mailto:chenwei@shanghaitech.edu.cn)).

Z. Deng, Y. Chen and B. Chen are with the Optoelectronic Device Laboratory, School of Information Science and Technology, ShanghaiTech University, Shanghai 201210, Peoples R China (e-mail: [dengzhuo@shanghaitech.edu.cn](mailto:dengzhuo@shanghaitech.edu.cn); [chenyj@shanghaitech.edu.cn](mailto:chenyj@shanghaitech.edu.cn); [chenbl@shanghaitech.edu.cn](mailto:chenbl@shanghaitech.edu.cn)).

D. Guo, H. Liu and J. Wu are with the Department of Electronic and Electrical Engineering, University College London, London WC1E 7JE, United Kingdom (e-mail: [daqian.guo.15@ucl.ac.uk](mailto:daqian.guo.15@ucl.ac.uk); [huiyun.liu@ucl.ac.uk](mailto:huiyun.liu@ucl.ac.uk); [jiang.wu@ucl.ac.uk](mailto:jiang.wu@ucl.ac.uk)).

Y. I. Mazur, Y. Maidaniuk M. Benamara and G. J. Salamo are with the Institute for Nanoscience and Engineering, University of Arkansas, Fayetteville, Arkansas 72701, United States (e-mail: [ymazur@uark.edu](mailto:ymazur@uark.edu); [ymaidani@uark.edu](mailto:ymaidani@uark.edu); [mourad@uark.edu](mailto:mourad@uark.edu); [salamo@uark.edu](mailto:salamo@uark.edu)).

\*These authors contributed equally to this work.

inter-subband transition in quantum wells, have been extensively investigated due to the feasibility of detection wavelength tuning. Quantum dot infrared photodetectors (QDIPs) are being considered as an alternative to QWIPs because of its sensitivity to normal incidence radiation, long carrier lifetime and potentially high operating temperature [2, 6, 7]. It has been theoretically predicted that QDIPs could have significantly better detectivity than QWIPs [3].

Mid-infrared (MIR) silicon photonics have recently attracted extensive attention same as the silicon photonics in the near-infrared telecommunication bands [8, 9]. Si platform working in MIR band offers an integrated solution for gas sensing, defense and medical applications at minimal cost. Therefore, as the key component of MIR silicon photonics systems, it would be desirable to monolithically grow MIR photodetectors on silicon substrate to integrate with other active and passive MIR devices. Moreover, by monolithic growth of infrared photodetector materials on large Si substrate one could substantially reduce the cost of focal plane array (FPA). Over the past decade, significant progress has been made in transferring MCT photodetectors and focal plane array (FPA) on Si substrates to enjoy the large Si substrate and reduce the cost that raise from the native substrates [4, 10]. Recently, Wu et al. have monolithically integrated InAs/GaAs QDIPs on Si substrate [11] for mid infrared detection, however, no qualitative characterization of responsivity, noise and detectivity has been reported in Wu's paper. Soon after, Wan et al. have demonstrated an *p-i-n* photodetector on GaAs-Si compliant substrate with optical response around 1310nm wavelength for telecommunication application, where the InAs quantum dots layers were used to absorb the near infrared light [12].

In this paper, we demonstrated and qualitatively characterized the first InAs/InGaAs/GaAs dots-in-the-well (DWELL) structure grown on Si substrate which operates in the MWIR range. This study benchmarks III-V MIR photodetectors on a Si substrate against these on native III-V substrates. The DWELL structure is one variation of the basic QDIP structure, which consists of an InAs quantum dots (QDs) layer sandwiched by two InGaAs quantum wells (QWs). This hybrid configuration combining the traditional QWIPs and QDIPs could offer important advantages such as lower dark current, stronger confinement of electrons and more flexibility of controlling the operation wavelength [13]. The DWELL photodetector studied in this work shows a lower dark current compared with that of Si based QDIPs, an optical response peak around 6.4  $\mu$ m, and a relatively high detectivity. Comparison between these Si-based DWELL devices to previous DWELL photodetectors grown on native III-V substrates is discussed. It is shown that these devices are very promising for future MIR silicon photonics and low cost FPA application.

## II. DEVICE DESIGN AND FABRICATION

Schematic diagram of the sample structure is shown in Fig. 1. The InAs/InGaAs/GaAs DWELL structures were directly grown on Si

(100) substrate using a solid-source Veeco Gen-930 molecular beam epitaxy system. The substrate has 4° offcut towards the [011] direction, in order to minimize the formation of anti-phase domains. Firstly, a 1000 nm n-type GaAs buffer layer was grown on Si substrate. Four repeats of dislocation filter layers (DFLs) comprised of InGaAs/GaAs superlattices (SLSs) were then grown. Fig. 2 (a) shows the bright-field transmission electron microscope (TEM) image of the buffer and DFLs layers. Due to the mismatch of lattice constant and thermal expansion coefficient between Si and GaAs, a large threading dislocation density (TDD) of  $\sim 10^9/\text{cm}^2$  was observed at the substrate/buffer interface. The InGaAs/GaAs DFLs was found to significantly inhibit the propagation of dislocation. After depositing four repeats of the DFLs, the TDD was quickly annihilated and reached a level of  $\sim 3 \times 10^6/\text{cm}^2$ .

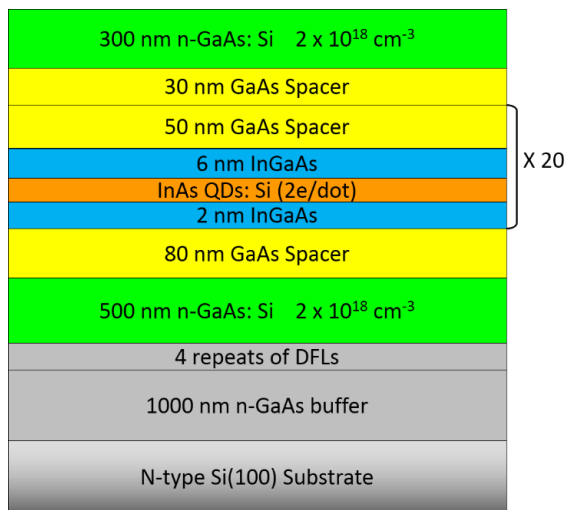
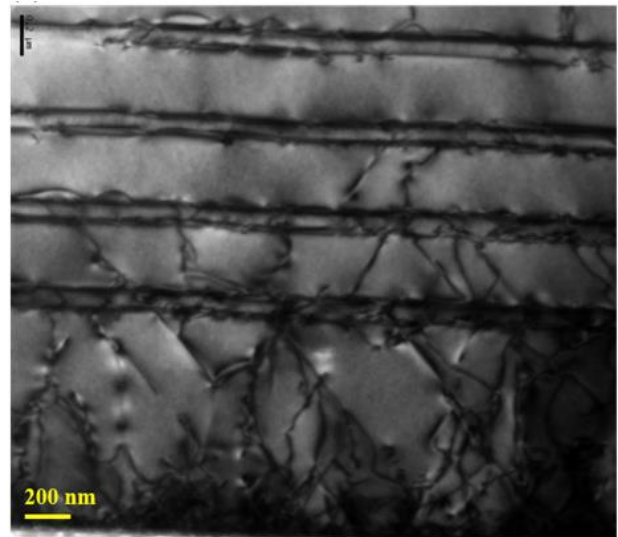


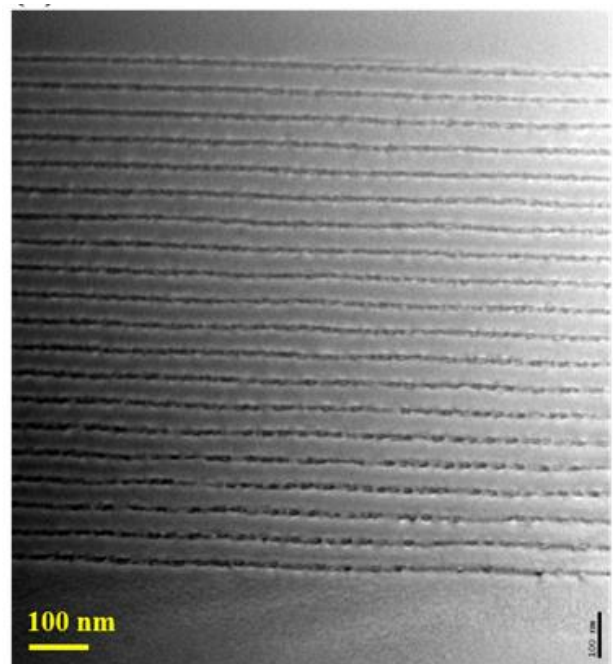
Fig. 1. Schematic layout of the InAs/InGaAs/GaAs DWELL structure.

After growing the buffer layer, a 500 nm n-type GaAs (Si-doped,  $2 \times 10^{18} \text{ cm}^{-3}$ ) bottom contact layer and 80 nm undoped GaAs spacer layer were grown. The DWELL active region consists of 20 periods of 50 nm undoped GaAs spacer layer, the InAs QD (Si-doped, 2 electrons/dot) layer sandwiched between two InGaAs quantum wells, with thickness of 6 nm and 2 nm respectively. The QD density is 400 dots/ $\mu\text{m}^2$ . As can be seen in Fig. 2 (b), the 20 periods DWELL active region is free of threading dislocation, which confirms the effective suppression of TDD by using the SLSs in the GaAs buffer on Si substrate. Finally, a 30 nm undoped GaAs spacer layer and 300 nm n-type GaAs (Si-doped,  $2 \times 10^{18} \text{ cm}^{-3}$ ) top contact layer were grown.

After the material growth, the DWELL sample was fabricated into a set of unpassivated mesa-isolated circular devices with nominal diameters ranging from 20  $\mu\text{m}$  to 500  $\mu\text{m}$ . Standard UV photolithography and wet chemical etching treatment ( $\text{H}_3\text{PO}_4$ :  $\text{H}_2\text{O}_2$ :  $\text{H}_2\text{O}$ =1:1:8) were utilized to define the mesa. Metal contacts of Ti/Au (50 nm/300 nm) were deposited at the top and bottom n<sup>+</sup>-GaAs layers by using electron beam evaporation and lift-off techniques.



(a)



(b)

Fig. 2. (a) Bright-field TEM image of the GaAs buffer layer and four repeats of the InGaAs/GaAs dislocation filter layers (DFLs); (b) Low-magnification bright-field TEM image of the 20 periods DWELL active region.

## III. RESULTS AND DISCUSSIONS

## A. Optical Characterization

The continuous-wave (CW) photoluminescence (PL) measurements were carried out in a variable-temperature closed-cycle helium cryostat, using the 532 nm line from a frequency doubled Nd:YAG (Neodymium doped Yttrium Aluminum Garnet) laser as the excitation source. The laser spot diameter was  $\sim 20$  mm and the optical excitation power was in the range of  $\sim 10^{-7}$  to  $10^2$  mW. The PL signal from the sample was dispersed by a monochromator and detected by a liquid nitrogen-cooled InGaAs photodiode detector array. Fig. 2(a) shows the PL spectra of the DWELL photodetector measured at 10 K under different excitation power. An emission peak at  $\sim 1.04$  eV is seen at the lowest excitation power  $I_{ex} = 25 \mu\text{W}/\text{cm}^2$ , which is possibly due to the interband transition from the QDs electron ground state to the hole ground state. A second emission peak at  $\sim 1.09$  eV related to the carrier transition from the electron excited state of QDs to the hole excited state arises in the high-energy side of the PL spectra with increasing excitation power, which can be explained by the state filling at high optical excitation power [11]. The asymmetric PL lineshape as shown in Fig. 2(a) is possibly attributed to the nonuniform size distribution of the QDs, which have been widely observed in InAs QDIP and DWELL structures [11, 14].

Fig. 2(b) demonstrates the temperature-dependent PL spectra measured at a fixed laser excitation power of  $10 \mu\text{W}/\text{cm}^2$  from 80 to 300 K. The extracted PL parameters associated with the QDs ground state transition, including integrated intensity, peak position and the Full-Width-at-Half-Maximum (FWHM) of the DWELL photodetector as a function of temperature are shown in Fig. 2(c).

With increasing temperature, the PL peak position presents a red-shift which does not follow the typical band gap shrinkage, and it is typically seen in InAs-based QDIP structures. This behavior indicates that the carriers undergo an inter-dots transfer from the smaller QDs with shallower energy levels to the larger QDs with deeper energy confinement under thermal excitation, which results in a lower interband emission energy and a red-shift of the PL peak position [11, 15, 16]. Such carrier transfer process could also be evidenced by the temperature dependence of the PL spectral linewidth as shown in Fig. 2(c). At low temperature, the FWHM of PL is mainly determined by the inhomogeneous QDs distribution, or in other words, it originates from the emission of QDs of many different sizes. A reduction of PL FWHM is observed until 180 K as temperature increases, which is due to the transfer of carriers from the smaller QDs to the larger QDs under thermal excitation. With the temperature further increases beyond 180 K, the broadening of PL FWHM is likely attributed to the electron-phonon scatter over QDs with different sizes [11, 16-18]. Furthermore, from Fig. 2(c) it is seen that as the temperature rises the PL integrated intensity decreases. In order to investigate the thermal quenching mechanism of carriers in the DWELL system, the Arrhenius plot of the integrated intensity is shown in Fig. 2 (d). The experimental data from 230 K onward can be fitted very well with the linear function, which yields an activation energy ( $E_A$ ) of  $\sim 153.8$  meV. This energy roughly corresponds to the excitation of electron from the confined states in the DWELL to the quasi-continuum states of the GaAs barrier, which suggests that the thermal escape of carriers is the dominant loss mechanism responsible for the rapid PL quenching at high temperature.

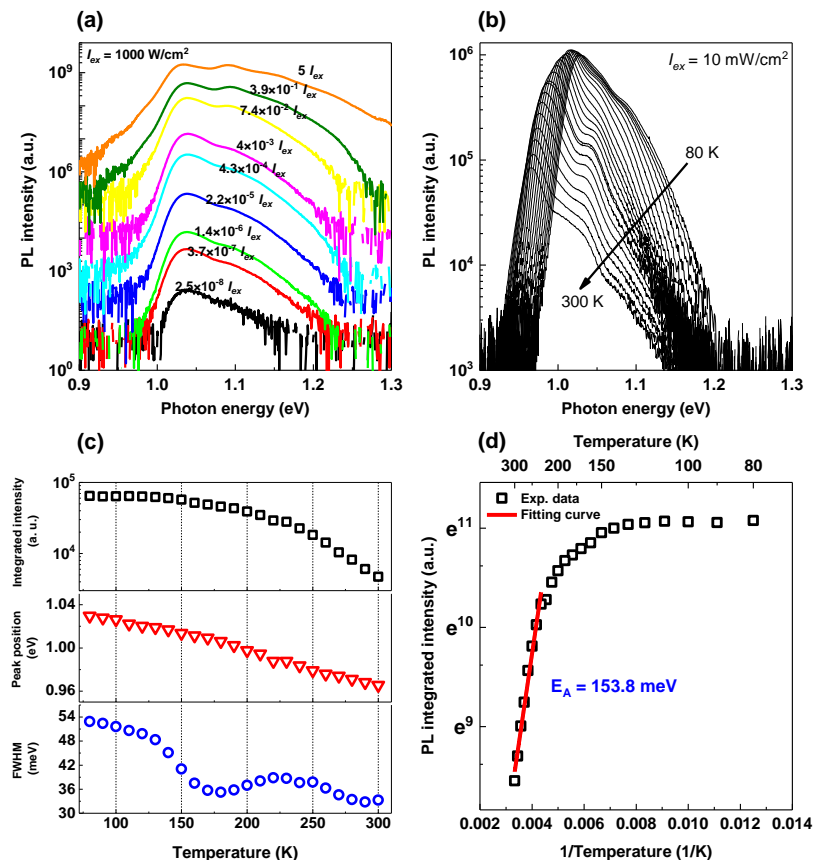


Fig. 3. (a) Excitation power-dependent PL spectra of the DWELL photodetector measured at 10 K.  $I_{ex} = 1000 \text{ W}/\text{cm}^2$ . (b) PL spectra as a function of temperature of the DWELL

photodetector measured from 80 to 300 K with an interval of 10 K. The excitation power was fixed at  $I_{ex} = 10 \text{ mW/cm}^2$ . (c) Temperature dependences of PL parameters (integrated intensity, peak position and FWHM) associated with the QDs ground state transition extracted from (b). (d) Arrhenius plot of the PL integrated intensity (open squares) from 80 K to 300 K. The solid line is the linear fit from 230 K to 300 K.

To further explore the optical properties of the DWELL photodetector grown on silicon substrate, time-resolved PL measurements were conducted using the 2 ps pulses of the 750 nm line from a mode-locked Ti:sapphire laser. The excitation density per pulse is  $6 \times 10^{11}$  photons/cm<sup>2</sup> and the optical pulse train frequency is 76 MHz. For detection of the transient PL signal, a monochromator with a Hamamatsu Synchroscan C5680 streak camera was exploited. The streak camera was equipped with an infrared enhanced S1 cathode possessing an overall time resolution of system  $\sim 15$  ps. Fig. 3(a) shows the time-resolved PL spectra measured at 10 K for different emission wavelengths. Apart from the emission at  $\sim 848$  nm (71 ps) from the wetting layer, all the PL decay processes have a relative long lifetime of over 450 ps. The extracted variation of PL

lifetime with wavelength is shown in Fig. 3(b), with the normalized PL spectrum measured at 10 K under the 532 nm excitation with a laser power of 5000 W/cm<sup>2</sup> is also plotted. The two main PL peaks corresponding to the QDs ground state and excited state transition have both shown a relatively long decay lifetime ( $> 800$  ps). In particular, the carrier lifetime associated with the QDs ground state transition measured at 1200 nm is  $\sim 1.52$  ns, which is  $\sim 17\%$  longer than that reported for the InAs/GaAs QDIP grown on Si substrate [11]. Thus, the incorporation of DWELL structure has ensured a long carrier relaxation time in the QDs, which demonstrates the potential for realization of inter-subband DWELL photodetectors with larger specific detectivity and higher operating temperature.

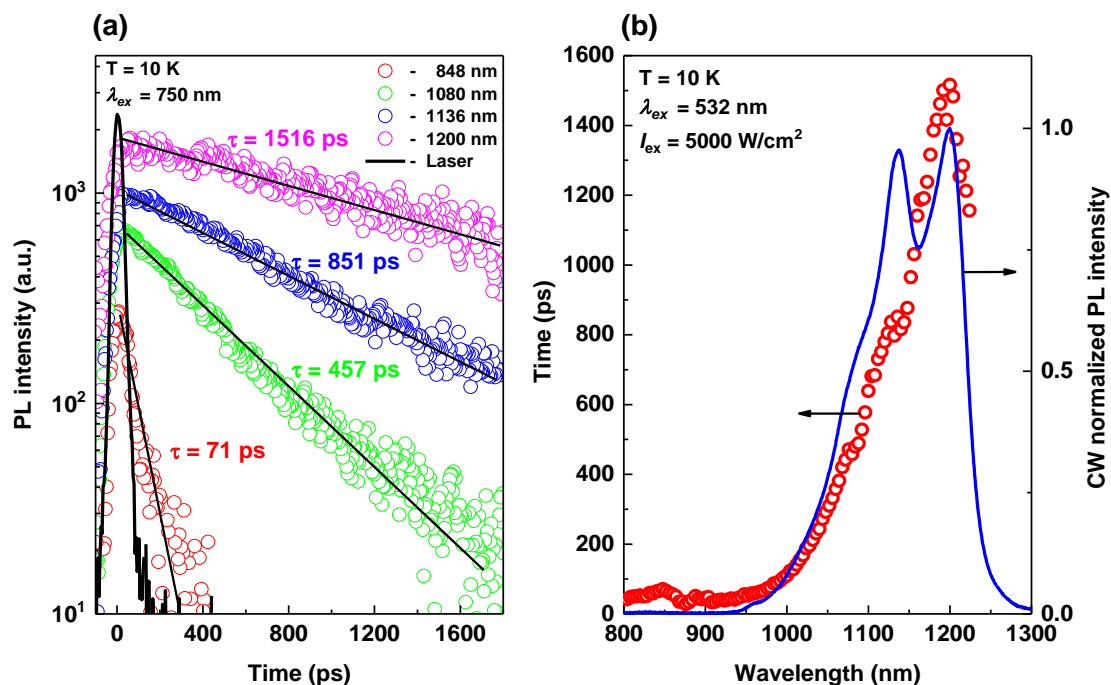


Fig. 4. (a) Time-resolved PL spectra measured from the DWELL photodetector at 10 K for different emission wavelengths: 848, 1080, 1136, and 1200 nm. (b) Estimated PL lifetime (open circles) versus wavelength. The blue curve is the normalized PL spectrum recorded at 10 K under the 532 nm line excitation with a laser power of 5000 W/cm<sup>2</sup>.

### B. Electrical Characterization

The dark current-voltage ( $I$ - $V$ ) characteristics of the DWELL photodetector device with diameter of 130  $\mu\text{m}$  were measured in the variable-temperature probe station from 77 to 300 K and the data were analyzed by a semiconductor device analyzer. The dark current  $I$ - $V$  characteristics are presented in Fig. 4. Note that the dark current measured at temperature higher than 180 K has exceeded the instrument compliance, and hence the data ranges are narrowed. With the temperature increasing from 77 K to 300 K, the dark current increases over 5 orders of magnitude from  $1.13 \times 10^{-6}$  mA to  $1.12 \times 10^{-1}$  mA under -1 V bias (the corresponding dark current density ( $J_d$ )

increases from  $8.5 \times 10^{-3}$  mA/cm<sup>2</sup> to  $8.4 \times 10^2$  mA/cm<sup>2</sup>). The dark current under 1 V bias at 77 K is  $2.69 \times 10^{-7}$  mA ( $J_d = 2.03 \times 10^{-3}$  mA/cm<sup>2</sup>). Compared with the dark current density of 2.8 mA/cm<sup>2</sup> (at 80 K and 1 V) measured from the similar InAs/GaAs QDIP grown on silicon substrate [11], the insertion of the two InGaAs QWs (DWELL structure) in the current QDIP has successfully reduced the dark current density by three orders of magnitude. It is also noted that the dark current curves as shown in Fig. 4 are asymmetric for positive and negative bias. This is possibly originated from the asymmetric band structure and nonuniform geometry of the quantum dot growth: carriers would experience different energy potentials depending on whether they travel towards the top or bottom contacts [11, 14].

Fig. 5 shows the Arrhenius plot extracted from the dark current

measurement under 0.5 V. A good linear fit is achieved from 77 K to 180 K, which yields a dark current activation energy ( $E_A$ ) of 151.4 meV. This energy is in good agreement with the activation energy extracted from the PL integrated intensity in Fig. 2 (d), which further supports our previous claim that the thermal escape of carriers take place from the electron quasi-Fermi level ( $E_F$ ) in the DWELL to the quasi-continuum states of GaAs barrier. Furthermore, the dependence of  $E_A$  on bias voltage is calculated and plotted in Fig. 6. Note that the discontinuity after  $\sim 2$  V is due to the fact that at 180 K the dark current has reached the instrument compliance when bias is larger than  $\sim 2$  V and thus the data are not included in the calculation. As the bias increases from 0 V in both positive and negative direction,  $E_A$  first demonstrates a rapid increase. It then experiences two stationary points at 0.58 V and  $-0.6$  V respectively, and declines slowly with further increase of bias. Such behaviors of dark current activation energy on bias were not seen in previous studies for InAs/InGaAs/GaAs DWELL photodetector grown on GaAs substrates, since only monotonic reduction of  $E_A$  were reported with increasing bias in both directions [14, 19-23]. We attempt to explain the anomalous bias dependence of  $E_A$  as follows: within the temperature range of 77–180 K, inter-dots carrier transfer process from smaller QDs to larger QDs is facilitated by thermalization, which is already evidenced by the temperature behavior of transition energy and linewidth from the PL measurement. With more carriers being localized in the larger QDs, where the electronic energy level relative to the GaAs conduction band edge is rather deep, an increase of activation energy is thus expected. In particular, the rapid reduction of PL FWHM from 130 K to 180 K as seen in Fig. 2(c) suggests a

rather fast rate of the inter-dots transfer process, which leads to the steep increment of  $E_A$  with bias. On the other hand, apart from the temperature effect, it should be further noted that the inter-dots carrier transfer is associated with bias voltage as well. The strong electric field induced by the applied bias would reduce the barrier height associated with the InGaAs QW and GaAs matrix of the DWELL structure, and consequently inter-dots carrier transfer would be enhanced via field-assisted tunneling with increasing bias [24, 25]. As shown in Fig. 6, the two stationary points of  $E_A$  observed at 0.58 V and  $-0.6$  V suggest that the carrier transfer process tends to be saturated and QDs of different sizes are nearly in equilibrium, where most of the lower lying states in the majority of QDs being filled. In this scenario, a further increase of bias voltage would elevate the electron quasi-Fermi level  $E_F$  towards the GaAs conduction band edge, and the energy required for the electrons to escape to the GaAs quasi-continuum levels, i.e.,  $E_A$ , would thus be reduced. Note that the decrement of activation energy slows down after  $\sim -1.5$  V, and a smaller slope is observed. This is due to the fact that deviation of dark current between different temperatures, i.e., curve spacing in Fig. 4, is getting smaller with increasing bias. The anomalous  $E_A$  dependence on bias also advices that field-assisted tunneling might be an important escape route for carrier at high bias voltage in this DWELL structure grown on Si substrate. This is an essential process for the realization of bias-tunable multicolor QDIP, since it provides a major pathway for the extraction of carriers photo-generated from the QDs ground state to the lower-lying excited states confined in the DWELL [25].

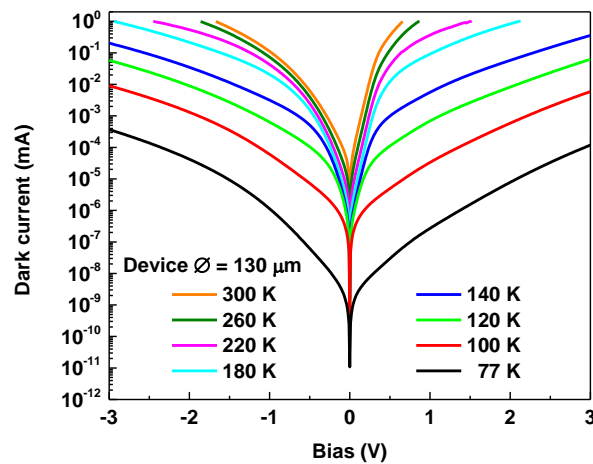


Fig. 5. Dark current-voltage ( $I$ - $V$ ) characteristic of the DWELL photodetector measured at different temperatures. The device diameter is 130  $\mu\text{m}$ .

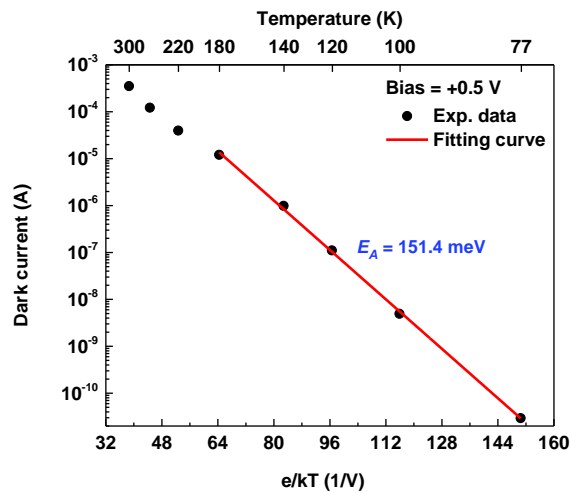


Fig. 6. Arrhenius plot of the dark current under 0.5 V bias. The solid line represents the linear fitting of the plot from 77 to 180 K.

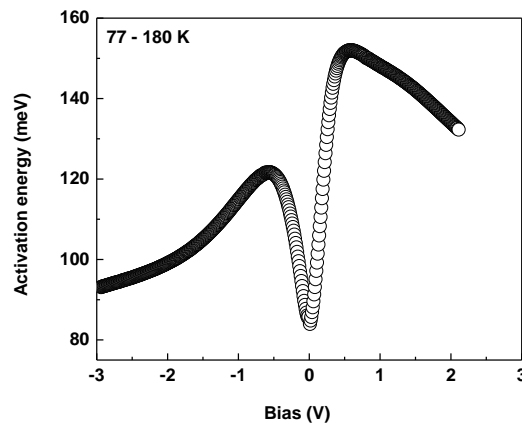


Fig. 7. Dark current activation energy ( $E_A$ ) calculated at different bias voltages.

### C. Optoelectronic Characterization

To further investigate the optoelectronic performances of the DWELL photodetectors, one DWELL device with diameter of 130  $\mu\text{m}$  was wire-bonded and loaded into a low-temperature cryostat for photoresponse and dark noise characterization. The photoresponse of the DWELL device was carried out with front-side illumination and without anti-reflection (AR) coating. The photocurrent and noise current were amplified by a low noise current preamplifier, and then analyzed and displayed by a fast Fourier transform (FFT) network spectrum analyzer. A NICOLET Fourier transform infrared spectrometer (FTIR) was used to measure the relative photoresponse of the DWELL sample. A standard blackbody source at 700  $^\circ\text{C}$  was used to measure the blackbody photoresponse and calibrate the relative responsivity. The blackbody responsivity versus bias at 77 K was measured and plotted in Fig. 7(a). Here the blackbody responsivity ( $BR$ ) is defined as the ratio between the output photocurrent and the input radiation power from the blackbody source

at 700  $^\circ\text{C}$ . As shown in Fig. 7(a), the blackbody responsivity curve presents an asymmetric lineshape for the positive and negative bias value, which is due to the same reason that gives rise to the asymmetry in dark current densities, i.e., asymmetric band structure that cause the electrons in the QDs to experience different barrier heights. The dark noise spectrum density measured at 77 K is shown in Fig. 7(b). For a relatively low bias ( $< \pm 0.5$  V), the noise measurement was limited by the noise floor of the instruments. It is clear that with increasing bias, both the blackbody responsivity and noise spectrum density increase. Fig. 7(c) plots the dependence of blackbody detectivity ( $BD^*$ ) on bias voltage. The blackbody detectivity is defined as [26]:

$$BD^* = \frac{BR\sqrt{A}}{S_n} \quad (1)$$

where  $BR$  represents the blackbody responsivity,  $A$  is the device area,  $S_n$  is the noise spectrum density. With the bias increases from 0.5 V to 1.25 V, the black responsivity increases a percentage of 605.2 %,

while the dark noise only increases a percentage of 27.5 %, thus the blackbody detectivity rises rapidly first with increasing bias. However, when the bias further increases from 1.25 V to 2 V, the rise of dark noise (447.1 %) prevails blackbody responsivity (243 %), which leads

to the plateau and drop of the blackbody detectivity observed after 1.25 V. The best performance under blackbody illumination is achieved at 1.25 V where the peak detectivity is  $2.11 \times 10^8 \text{ cm} \cdot \text{Hz}^{1/2} / \text{W}$ , as shown in Fig. 7(c).

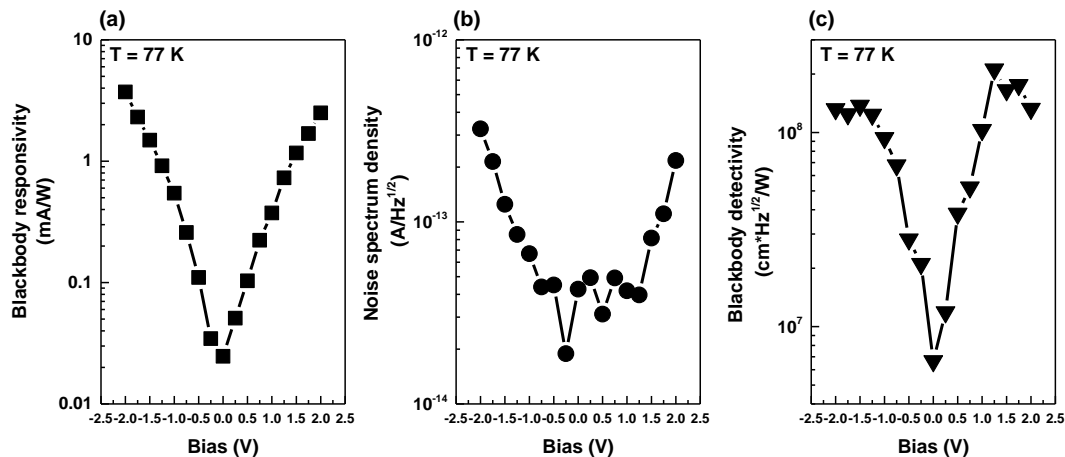


Fig. 8. Bias voltage dependences of: (a) Blackbody responsivity; (b) Noise spectrum density; and (c) Blackbody detectivity measured at 77 K.

Fig. 8(a) and (b) shows the calibrated absolute responsivity of the DWELL photodetector under  $\pm 2 \text{ V}$ ,  $\pm 1 \text{ V}$  and  $\pm 0.5 \text{ V}$  bias at 77 K, respectively. The sharp peaks observed at  $\sim 8.6 \mu\text{m}$  in both positive and negative bias are considered as artifacts and should be discarded. As can be seen in Fig. 8(b), the responsivity of the DWELL photodetector peaks at  $14.67 \text{ mA/W}$  at  $7.09 \mu\text{m}$  ( $\sim 175 \text{ meV}$ ) under  $-2 \text{ V}$  bias, and it reduces to  $1.97 \text{ mA/W}$  and  $0.39 \text{ mA/W}$  when bias decreases to  $-1 \text{ V}$  and  $-0.5 \text{ V}$ , respectively. The corresponding peak wavelength positions are  $5.5 \mu\text{m}$  ( $\sim 225 \text{ meV}$ ) and  $5.45 \mu\text{m}$  ( $\sim 228 \text{ meV}$ ). Similarly for the forward bias, the maximum responsivity measured under  $2 \text{ V}$ ,  $1 \text{ V}$  and  $0.5 \text{ V}$  are found at  $10.9 \text{ mA/W}$ ,  $1.29 \text{ mA/W}$  and  $0.46 \text{ mA/W}$ , respectively. The corresponding wavelengths are  $6.39 \mu\text{m}$  ( $\sim 194 \text{ meV}$ ),  $5.85 \mu\text{m}$  ( $\sim 212 \text{ meV}$ ) and  $5.52 \mu\text{m}$  ( $\sim 225 \text{ meV}$ ) respectively. We notice that these photoresponse energies, which correspond to the inter-subband transition from QDs electron ground state to the quasi-continuum states of the GaAs matrix, are larger than that in the InAs/GaAs QDIP grown on Si substrate without the insertion of the two InGaAs QWs. For instance, the peak photoresponse at  $1 \text{ V}$  is  $\sim 6.5 \mu\text{m}$  ( $\sim 191 \text{ meV}$ ) [15], which is  $21 \text{ meV}$  smaller than the current DWELL sample. On the other hand, the PL emission energy associated with the QDs electron ground state transition observed in the same InAs/GaAs QDIP structure showed blue-shift compared with the current DWELL structure ( $1036 \text{ nm}$  v.s.  $1200 \text{ nm}$ ). These results jointly suggest the additional InGaAs QWs sandwiched between the InAs QDs have lowered the ground state levels of electrons and holes in the QDs, leading to a blue-shift of inter-subband detection wavelength. Future works will be focused on optimizing the thickness and composition of the QWs layers to improve the performance and tune the detection wavelength of the DWELL device. From Fig. 8 it can be seen the responsivity

intensities are asymmetric between negative and positive bias, which is possibly arisen from the asymmetric growth of the self-assembled QDs in the Stranski-Krastanov mode [11, 27]. Moreover, for both positive and negative bias, the photoresponse peaks shift to the longer wavelength (red-shift) with increasing bias. An energy shift of  $\sim 31 \text{ meV}$  is observed for positive bias whereas a larger shift of  $\sim 53 \text{ meV}$  is observed for negative bias. The bias-tunability of photoresponse could be found in many InAs-based DWELL photodetector structures, which can be attributed to the quantum confined Stark effect (QCSE) [28, 29]. It should be noted that the peak response energies are significantly larger than the dark current activation energy ( $E_A$ ) obtained above. For instance, the photoresponse peak energy under  $0.5 \text{ V}$  is  $\sim 225 \text{ meV}$ , which is  $\sim 74 \text{ meV}$  larger than the  $E_A$  at the same bias ( $151.4 \text{ meV}$ ). Difference in energy between the dark current activation and inter-subband photoresponse process have also been reported previously for similar InAs/InGaAs/GaAs DWELL photodetectors [24, 29, 30]. We believe this discrepancy is due to the fact the electron quasi-Fermi level lies above the fully-filled QDs ground states.

Based on the previous studies for similar DWELL structures and the energetic data obtained from interband PL, dark current fitting and photoresponse measurements, we could deduce experimentally the energy band profile of our DWELL photodetector structure as depicted in Fig. 9. The conduction band offset between the GaAs spacer layer and InAs QDs is estimated to be  $250\text{--}297 \text{ meV}$  according to semi-empirical calculations reported by Krishna *et al* and Dixit *et al*. [2, 30]. Similarly, the barrier height between InGaAs QWs and GaAs spacer layers is  $194 \pm 10 \text{ meV}$  [30]. These energy schemes support our previous attribution of photoresponse peak energy to the inter-subband transition from the QDs ground states to the quasi-continuum levels.

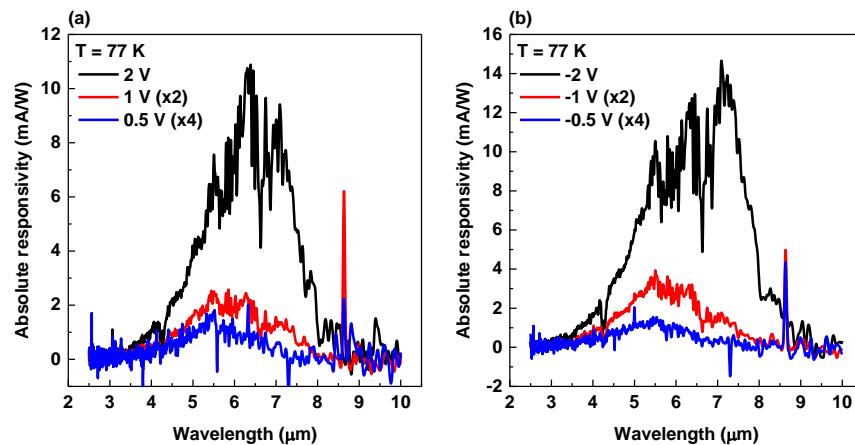


Fig. 9. Absolute responsivity of the DWELL photodetector measured under (a) 2 V, 1 V and 0.5 V; and (b) -2 V, -1 V and -0.5 V at 77 K.

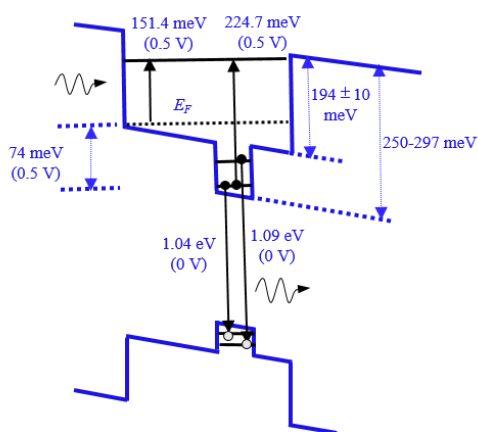


Fig. 10. Experimentally obtained conduction and valence band profile of the DWELL structure. The one-way arrows represent upward (photoresponse, dark current) and downward (PL) transition from the DWELL structure, whereas the two-way arrows depict the estimated barrier height, conduction band offset and the energy separation between QD ground state and electron quasi-Fermi level  $E_F$  (dashed black line). The solid black lines label the energy states related to different transition processes.

Finally, the absolute responsivity and the noise spectrum density are utilized to calculate the specific detectivity ( $D^*$ ) of the DWELL photodetector under different bias voltages. The specific detectivities at 77 K under  $\pm 2$  V bias are shown in Fig. 10. The best performance is achieved at 2 V, where the peak specific detectivity is  $5.78 \times 10^8$   $\text{cm} \cdot \text{Hz}^{1/2} / \text{W}$  at 6.4  $\mu\text{m}$  with the corresponding responsivity of 10.9  $\text{mA/W}$ . The specific detectivity reported recently in photodetectors with similar DWELL structures grown on GaAs substrates are shown in Table. 1. Compared with the best device reported by Ling et al. with the confinement enhanced AlGaAs barrier layers which achieved  $D^*$  of  $\sim 1 \times 10^{10}$   $\text{cm} \cdot \text{Hz}^{1/2} / \text{W}$  [31], our DWELL photodetector is  $\sim 20$  times lower in  $D^*$ . Nevertheless, we also noted that the dark current density reported in their device is  $3.8 \times 10^{-1}$   $\text{mA/cm}^2$  (at -1 V and 77 K), which is much larger than that in our device ( $8.5 \times 10^{-3}$   $\text{mA/cm}^2$ ) measured at same conditions. This result is encouraging and confirms that the silicon-based DWELL photodetector has a promising development potential in silicon-based MWIR applications. The reason that the DWELL device shows lower  $D^*$  performance than Ling's device [31] is mainly due to the lower responsivity in the current structure. Therefore, some future works on these DWELL QDIP devices are still needed to improve quantum efficiency and

tune the peak detection wavelength by optimizing device structure and material growth condition.

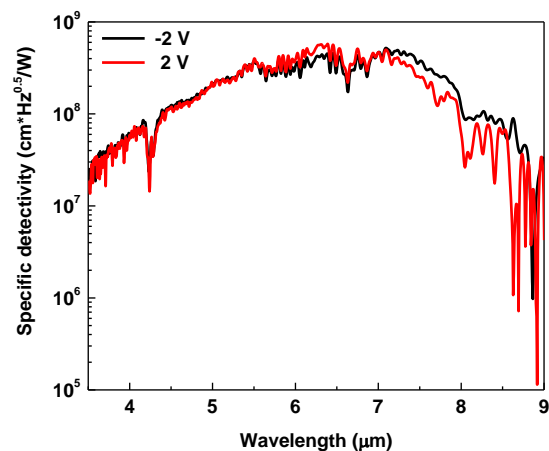


Fig. 11. Specific detectivity of the DWELL photodetector calculated at different wavelength under  $\pm 2$  V bias at 77 K.

TABLE I  
COMPARISON OF PERFORMANCE OF SIMILAR DWELL PHOTODETECTORS

| Works                       | Active region           | Substrate | Peak $D^*$ (cm·Hz <sup>1/2</sup> /W) | Peak $\lambda$ ( $\mu$ m) |
|-----------------------------|-------------------------|-----------|--------------------------------------|---------------------------|
| Ling et al. [31]            | InAs/InGaAs/AlGaAs      | GaAs      | $1 \times 10^{10}$ (-0.9 V, 77 K)    | 8                         |
| H. Ghadi et al. [6]         | InAs/InGaAs/GaAs        | GaAs      | $4.1 \times 10^9$ (-1 V, 87 K)       | 7.3                       |
| A. G. U. Perera et al. [32] | InAs/InGaAs/GaAs        | GaAs      | $1.4 \times 10^9$ (-2 V, 78 K)       | 5                         |
| This work                   | InAs/InGaAs/GaAs        | Si        | $5.8 \times 10^8$ (2 V, 77 K)        | 6.4                       |
| Srinivasan et al. [23]      | InAs/InGaAs/GaAs/AlGaAs | GaAs      | $4 \times 10^8$ (2 V, 77 K)          | 4.4                       |

#### IV. CONCLUSIONS

In summary, we have demonstrated the first InAs/InGaAs/GaAs DWELL photodetector monolithically grown on silicon substrate. The incorporation of the DWELL structure in the InAs-based QDIP ensured a long carrier lifetime of 1.52 ns and three orders of magnitudes reduction in dark current densities, which suggested that a high-quality DWELL structure could be obtained on silicon substrate. A peak specific detectivity of  $5.78 \times 10^8$  cm·Hz<sup>1/2</sup>/W under 2 V bias at 6.4  $\mu$ m and 77 K was achieved in these DWELL photodetectors with the corresponding responsivity of 10.9 mA/W. Our work shows that the performance of these III-V DWELL MWIR photodetectors directly grown on silicon substrate are very promising for future cost-effective silicon photonics application.

#### REFERENCES

- [1] A. Rogalski, "Infrared detectors: status and trends," *Progress in Quantum Electronics*, vol. 27, pp. 59-210, 2003/01/01/ 2003.
- [2] S. Krishna, "Quantum dots-in-a-well infrared photodetectors," *Infrared Physics & Technology*, vol. 47, pp. 153-163, 2005/10/01/ 2005.
- [3] P. Martyniuk and A. Rogalski, "Quantum-dot infrared photodetectors: Status and outlook," *Progress in Quantum Electronics*, vol. 32, pp. 89-120, 2008.
- [4] V. M. Bazovkin, S. A. Dvoretzky, A. A. Guzev, A. P. Kovchavtsev, D. V. Marin, V. G. Polovinkin, et al., "High operating temperature SWIR p+n FPA based on MBE-grown HgCdTe/Si(013)," *Infrared Physics & Technology*, vol. 76, pp. 72-74, 2016/05/01/ 2016.
- [5] C. Downs and T. Vanderveelde, "Progress in Infrared Photodetectors Since 2000," *Sensors*, vol. 13, p. 5054, 2013.
- [6] H. Ghadi, S. Sengupta, S. Shetty, A. Manohar, A. Balgarkashi, S. Chakrabarti, et al., "Comparison of Three Design Architectures for Quantum Dot Infrared Photodetectors: InGaAs-Capped Dots, Dots-in-a-Well, and Submonolayer Quantum Dots," *Ieee Transactions on Nanotechnology*, vol. 14, pp. 603-607, Jul 2015.
- [7] S. Wolde, Y.-F. Lao, A. G. Unil Perera, Y. H. Zhang, T. M. Wang, J. O. Kim, et al., "Noise, gain, and capture probability of p-type InAs-GaAs quantum-dot and quantum dot-in-well infrared photodetectors," *Journal of Applied Physics*, vol. 121, p. 244501, 2017.
- [8] A. Spott, E. J. Stanton, N. Volet, J. D. Peters, J. R. Meyer, and J. E. Bowers, "Heterogeneous Integration for Mid-Infrared Silicon Photonics," *IEEE Journal of Selected Topics in Quantum Electronics*, 2017.
- [9] H. Lin, Z. Luo, T. Gu, L. C. Kimerling, K. Wada, A. Agarwal, et al., "Mid-infrared integrated photonics on silicon: a perspective," *Nanophotonics*.
- [10] E. P. G. Smith, G. M. Venzor, Y. Petraitis, M. V. Liguori, A. R. Levy, C. K. Rabkin, et al., "Fabrication and Characterization of Small Unit-Cell Molecular Beam Epitaxy Grown HgCdTe-on-Si Mid-Wavelength Infrared Detectors," *Journal of Electronic Materials*, vol. 36, pp. 1045-1051, August 01 2007.
- [11] J. Wu, Q. Jiang, S. Chen, M. Tang, Y. I. Mazur, Y. Maidaniuk, et al., "Monolithically Integrated InAs/GaAs Quantum Dot Mid-Infrared Photodetectors on Silicon Substrates," *ACS Photonics*, vol. 3, pp. 749-753, 2016/05/18 2016.
- [12] Y. Wan, Z. Zhang, R. Chao, J. Norman, D. Jung, C. Shang, et al., "Monolithically integrated InAs/InGaAs quantum dot photodetectors on silicon substrates," *Optics Express*, vol. 25, pp. 27715-27723, 2017/10/30 2017.
- [13] Y. Wei, W. Ma, J. Huang, Y. Zhang, Y. Huo, K. Cui, et al., "Very long wavelength quantum dot infrared photodetector using a modified dots-in-a-well structure with AlGaAs insertion layers," *Applied Physics Letters*, vol. 98, p. 103507, 2011.
- [14] Z. M. Ye, J. C. Campbell, Z. H. Chen, E. T. Kim, and A. Madhukar, "InAs quantum dot infrared photodetectors with In<sub>0.15</sub>Ga<sub>0.85</sub>As strain-relief cap layers," *Journal of Applied Physics*, vol. 92, pp. 7462-7468, Dec 2002.
- [15] D. Pal, V. G. Stoleru, E. Towe, and D. Firsov, "Quantum dot-size variation and its impact on emission and absorption characteristics: An experimental and theoretical modeling investigation," *Japanese Journal of Applied Physics Part 1-Regular Papers Short Notes & Review Papers*, vol. 41, pp. 482-489, Feb 2002.
- [16] Y. I. Mazur, B. L. Liang, Z. M. Wang, G. G. Tarasov, D. Guzun, and G. J. Salamo, "Development of continuum states in photoluminescence of self-assembled InGaAs/GaAs quantum dots," *Journal of Applied Physics*, vol. 101, p. 6, Jan 2007.
- [17] M. C. Tang, S. M. Chen, J. Wu, Q. Jiang, V. G. Drogan, M. Benamara, et al., "1.3- $\mu$ m InAs/GaAs quantum-dot lasers monolithically grown on Si substrates using InAlAs/GaAs dislocation filter layers," *Optics Express*, vol. 22, pp. 11528-11535, May 2014.
- [18] R. Heitz, M. Veit, N. N. Ledentsov, A. Hoffmann, D. Bimberg, V. M. Ustinov, et al., "Energy relaxation by multiphonon processes in InAs/GaAs quantum dots," *Physical Review B*, vol. 56, pp. 10435-10445, Oct 1997.
- [19] H. Ghadi, S. Adhikary, A. Agarwal, and S. Chakrabarti, "Tuning in spectral response due to rapid thermal annealing on dot-in-a-well infrared photodetectors," *Superlattices and Microstructures*, vol. 65, pp. 106-112, Jan 2014.
- [20] A. V. Barve, S. Sengupta, J. O. Kim, J. Montoya, B. Klein, M. A. Shirazi, et al., "Barrier Selection Rules for Quantum Dots-in-a-Well Infrared Photodetector," *Ieee Journal of Quantum Electronics*, vol. 48, pp. 1243-1251, Oct 2012.

- [21] A. Barve, J. Y. Shao, Y. D. Sharma, T. E. Vandervelde, K. Sankalp, S. J. Lee, *et al.*, "Resonant Tunneling Barriers in Quantum Dots-in-a-Well Infrared Photodetectors," *Ieee Journal of Quantum Electronics*, vol. 46, pp. 1105-1114, Jul 2010.
- [22] S. Raghavan, P. Rotella, A. Stintz, B. Fuchs, S. Krishna, C. Morath, *et al.*, "High-responsivity, normal-incidence long-wave infrared ( $\lambda$  similar to 7.2  $\mu$  m) InAs/In<sub>0.15</sub>Ga<sub>0.85</sub>As dots-in-a-well detector," *Applied Physics Letters*, vol. 81, pp. 1369-1371, Aug 2002.
- [23] T. Srinivasan, P. Mishra, S. K. Jangir, R. Raman, D. V. S. Rao, D. S. Rawal, *et al.*, "Molecular Beam Epitaxy growth and characterization of silicon - Doped InAs dot in a well quantum dot infrared photo detector (DWELL-QDIP)," *Infrared Phys. Technol.*, vol. 70, pp. 6-11, May 2015.
- [24] L. Hoglund, K. F. Karlsson, P. O. Holtz, H. Pettersson, M. E. Pistol, Q. Wang, *et al.*, "Energy level scheme of InAs/In<sub>x</sub>Ga<sub>1-x</sub>As/GaAs quantum-dots-in-a-well infrared photodetector structures," *Physical Review B*, vol. 82, p. 7, Jul 2010.
- [25] S. Krishna, D. Forman, S. Annamalai, P. Dowd, P. Varangis, T. Tumolillo, *et al.*, "Demonstration of a 320x256 two-color focal plane array using InAs/InGaAs quantum dots in well detectors," *Applied Physics Letters*, vol. 86, p. 3, May 2005.
- [26] B. Chen, W. Jiang, J. Yuan, A. L. Holmes, and B. M. Onat, "SWIR/MWIR InP-based PIN photodiodes with InGaAs/GaAsSb type-II quantum wells," *IEEE Journal of Quantum Electronics*, vol. 47, pp. 1244-1250, 2011.
- [27] W. Q. Ma, X. J. Yang, M. Chong, T. Yang, L. H. Chen, J. Shao, *et al.*, "Voltage tunable two-color InAs/GaAs quantum dot infrared photodetector," *Applied Physics Letters*, vol. 93, p. 3, Jul 2008.
- [28] I. Sandall, J. S. Ng, J. P. R. David, C. H. Tan, T. Wang, and H. Liu, "1300 nm Wavelength InAs Quantum Dot Photodetector Grown on Silicon," *Optics Express*, vol. 20, pp. 10446-10452, 2012/05/07 2012.
- [29] P. Aivaliotis, N. Vukmirovic, E. A. Zibik, J. W. Cockburn, D. Indjin, P. Harrison, *et al.*, "Stark shift of the spectral response in quantum dots-in-a-well infrared photodetectors," *Journal of Physics D-Applied Physics*, vol. 40, pp. 5537-5540, Sep 2007.
- [30] V. K. Dixit, S. K. Khamari, C. Tyagi, S. D. Singh, S. Porwal, R. Kumar, *et al.*, "Evaluation of electronic transport properties and conduction band offsets of asymmetric InAs/In<sub>x</sub>Ga<sub>1-x</sub>As/GaAs dot-in-well structures," *Journal of Physics D-Applied Physics*, vol. 45, p. 12, Sep 2012.
- [31] H. S. Ling, S. Y. Wang, C. P. Lee, and M. C. Lo, "High quantum efficiency dots-in-a-well quantum dot infrared photodetectors with AlGaAs confinement enhancing layer," *Applied Physics Letters*, vol. 92, p. 193506, 2008.
- [32] A. G. U. Perera, Y. F. Lao, S. Wolde, Y. H. Zhang, T. M. Wang, J. O. Kim, *et al.*, "InAs/GaAs quantum dot and dots-in-well infrared photodetectors based on p-type valence-band intersublevel transitions," *Infrared Physics & Technology*, vol. 70, pp. 15-19, May 2015.